Cell-Laden Bioink Circulation-Assisted Inkjet-Based Bioprinting to Mitigate Cell Sedimentation and Aggregation

Jiachen Liu,[1] Md Shahriar,[1] Heqi Xu,[1] Changxue Xu[1,*]

[1] Department of Industrial, Manufacturing, and Systems Engineering, Texas Tech University, Lubbock, Texas 79409, USA

[*] Corresponding Author
Changxue Xu, Department of Industrial, Manufacturing, and Systems Engineering, Texas Tech University, Lubbock, Texas, 79409, USA, Tel: 806-834-6014; Email: changxue.xu@ttu.edu

Abstract
3D bioprinting precisely deposits picolitre bioink to fabricate functional tissues and organs in a layer-by-layer manner. The bioink used for 3D bioprinting incorporates living cells. During printing, cells suspended in the bioink sediment to form cell aggregates through cell-cell interaction. The formation of cell aggregates due to cell sedimentation have been widely recognized as a significant challenge to affect the printing reliability and quality. This study has incorporated the active circulation into the bioink reservoir to mitigate cell sedimentation and aggregation. Force and velocity analysis were performed, and a circulation model has been proposed based on iteration algorithm with the time step for each divided region. It has been found that (1) the comparison of the cell sedimentation and aggregation with and without the active bioink circulation has demonstrated high effectiveness of active circulation to mitigate cell sedimentation and aggregation for the bioink with both a low cell concentration of 1×10^6 cells/ml and a high cell concentration of 5×10^6 cells/ml; and (2) the effect of circulation flow rate on cell sedimentation and aggregation has been investigated, showing that large flow rate results in slow increments in effectiveness. Besides, the predicted mitigation effectiveness percentages on cell sedimentation by the circulation model generally agrees well with the experimental results. In addition, the cell viability assessment at the recommended maximum flow rate of 0.5 ml/min has demonstrated negligible cell damage due to the circulation. The proposed active circulation approach is an effective and efficient approach with superior performance in mitigating cell sedimentation and aggregation, and the resulting knowledge is easily applicable to other 3D bioprinting techniques significantly improving printing reliability and quality in 3D bioprinting.

Keywords
cell aggregation; cell sedimentation; bioink circulation; cell concentration; mitigation

1. Introduction
After several decades of development, three-dimensional (3D) printing, often referred to as additive manufacturing, has been widely applied to a variety of engineering fields, such as aerospace engineering, civil engineering, biomedical engineering, to name a few [1-3]. As one of the ramifications, 3D bioprinting has found wide applications in tissue engineering and regenerative medicine [4, 5]. It is based on layer-by-layer fabrication using bioink as the building blocks to fabricate functional bio-structures, which offers the opportunity to alleviate the shortage problem of tissues and organs [6]. Among three major bioprinting techniques, namely inkjet-based

[7-9], extrusion-based [10-12], and laser-assisted printing [13-15], inkjet-based printing has been favored due to some important merits, such as precise controllability on droplet size and deposition, easy scale-up, high printing speed and resolution, and high post-printing cell viability, to name a few [16, 17]. The bioink used for 3D bioprinting generally comprises of two main components: biological materials and living cells. Biological materials mimic natural extracellular matrix (ECM) to promote cell attachment, proliferation and migration [18]. Commonly applied biological materials are natural or synthetic polymers, such as alginate [19], collagen [20], gelatin methacrylate [21], fibroin [22], polyethylene glycol [8], to name a few. There are various living cells utilized in inkjet-based bioprinting, such as D1 murine mesenchymal stem cells [23], adult rat retinal ganglion cells [24], MCF-7 breast cancer cells [25], to name a few. 3D artificial tissue models have been successfully fabricated using inkjet-based bioprinting, such as vascular-like structures [8], skin [26], and cartilage [27].

The bioink used for 3D bioprinting incorporates living cells. During printing, the buoyant force of the cells provided by the bioink is always less than the gravitational force because of the density difference, resulting in cell sedimentation to the bottom of the bioink reservoir [28, 29]. As a result, the cell concentration at the bottom of the bioink reservoir increases significantly. Once the distance between adjacent cells becomes small enough, the cells adhere with each other to form the cell aggregates through cell-cell interaction. Cell sedimentation-induced cell aggregation has been extensively reported as a significant challenge to affect the printing reliability and quality. Lee *et al.* [30] reported that the accumulated cell aggregation brought high risks of nozzle clogging with odd jetting performance. Pepper *et al.* [23] investigated the number of deposited cells per pattern over time using a thermal inkjet bioprinter. It was reported that the polystyrene latex bead output profile increased monotonically, while the D1 murine stem cell output profile increased and then decreased due to cell aggregation and the cartridge surfaces. Similarly, Lorber *et al.* [24] reported that the retained cell population was reduced by 33% for the retinal ganglion cells and 57% for the glial cells, respectively, during investigation of the effects of printing process on cell viability and neurite outgrowth. The main reason was the cell sedimentation-induced cell aggregation and the associated adhesion to the inner surface of the tube and piezoelectric inkjet dispenser.

To mitigate cell sedimentation and the resultant cell aggregation in 3D bioprinting, some researchers have made contributions. These approaches are categorized into two types: bioink property manipulation and active stirring. For the bioink property manipulation, Chahal *et al.* [25] added Ficoll PM400 at concentration of 10–15% (w/v) into the bioink containing MCF-7 breast cancer with a concentration of 5×10^5 cells/ml to achieve the nearly neutral buoyance for the suspended cells during drop-on-demand (DOD) inkjet printing. It was reported that the post-38 printing average number of cells was significantly improved with a deviation of 41% using 10% (w/v) Ficoll PM400 compared to that of 110% without Ficoll PM400. Moreover, the normalized absorbance reflecting the cell viability remained 0.97–1.11 after 48 hours indicating no significant adverse effects of the added Ficoll PM400 on the cell viability. Similarly, Hewes *et al.* [31] implemented a piezoelectric inkjet nozzle to fabricate microvessels using the bioink containing 0.7% (w/v) alginate and human umbilical vein endothelial cells with a concentration of 5×10^6 cells/ml. 5% (w/v) bovine serum albumin was added into the bioink to achieve the nearly neutral buoyancy and the cell sedimentation and aggregation was suppressed. It was reported that the printing reliability was significantly improved with continuous 1-hour printing without nozzle

clogging. For the active stirring, Dudman *et al.* [32] introduced two agitator designs into DOD inkjet printing including a shaft-driven axial flow impeller and an internally mounted cylindrical neodymium magnet. It was reported that for both the mesenchymal stromal cells and chondrocyte cells, the agitators substantially reduced the cell aggregation within the 2 hours of printing. The normalized cells per droplet (NCPD) indicating the printing performance for the agitated inkjet printing system were stable in the range of 0.4–0.5. However, the NCPD for the inkjet printing system without agitation decreased significantly from 0.5 to 0 within 75 minutes, after which there were no cells within the droplets. The viability, metabolic activity and morphology of both types of cells were not found to be significantly affected by the agitation process. Likewise, Parsa *et al.* [33] introduced a magnetic-driven stir bar to the bioink reservoir during inkjet printing of the bioink containing Hep G2 hepatoma cells at a density of 5×10^5 cells/ml. The cell-laden bioink was actively agitated for 5 seconds every 2 minutes to alleviate cell sedimentation and aggregation. However, the dispersion was locally around the stir bar and the even dispersion of cells within the whole reservoir was not realized. The measured cell number varied significantly from 15% to 544% of the approximated 7,000 cells in the control case, indicating the poor repeatability. Moreover, the continuous stirring at a speed of 120 rpm was reported to decrease the cell viability from around 99% to 75% after 50-minute printing.

Although the aforementioned mitigation approaches are proved to be effective, there are some critical issues. For the bioink property manipulation, it requires careful formulation to reduce the difference between the mass density of cells and bioink. Moreover, it is extremely difficult to accommodate multiple cell types in the bioink to simultaneously achieve neutral buoyancy because different types of cells have different cell mass densities. For the active stirring, since it is mechanical mixing-based, the shear stress directly imposed on the cells may result in cell damage, especially for some types of cells that are sensitive to mechanical stresses. Thus, it is critical to investigate new effective and efficient mitigation approaches. In this study, we propose a bioink circulation-assisted inkjet printing system to mitigate the cell sedimentation and the resultant cell aggregation without manipulating bioink properties. The rest of this paper is organized as follows: Section 2 describes the materials, experimental setup and conditions, quantification methods, and force and velocity analysis. Section 3 proposes a circulation model for cell sedimentation, demonstrates the effectiveness of the proposed bioink circulation approach for both low and high cell concentration bioink, and investigates the effects of circulation flow rate on mitigation of cell sedimentation and aggregation. Section 4 discusses some issues, concerns, and cell viability. Section 5 summarizes the main conclusions and proposes some future work.

2. Materials and methods

2.1. Bioink preparation

The prepared bioink consists of ECM and living cells. The ECM is a 3D network consisting of macromolecules and minerals (e.g., collagen, enzymes, etc.) which provides structural and biochemical support to surround cells. Sodium alginate (NaAlg) used in this study has been widely utilized as the ECM in 3D bioprinting and tissue engineering to facilitate cellular attachment, proliferation, and differentiation due to its biocompatibility, biodegradation, hydrophilicity, and low cost [34, 35]. NIH 3T3 mouse fibroblasts (ATCC, Rockville, MD), as the most common cells of connective tissues in mammal, were selected as the model cell in this study [36, 37].

The NaAlg solution was prepared by dissolving NaAlg powder (Sigma-Aldrich, St. Louis, MO) into the Dulbecco's Modified Eagles Medium (DMEM; Sigma-Aldrich, St. Louis, MO) with a concentration of 0.5% (w/v). The NIH 3T3 mouse fibroblasts were cultured in Dulbecco's Modified Eagles Medium (DMEM; Sigma-Aldrich, St. Louis, MO) supplemented with 10% Bovine Calf Serum (BCS; Hyclone, Manassas, VA) and 1% antibiotic/antimycotic solution (Corning, Manassas, VA) in a humidified 5% CO_2 incubator at 37 ℃. The culture medium was changed every other day. The cells cultured in the flasks were detached by adding 0.25% Trypsin/EDTA (Sigma-Aldrich) for 5-minute incubation. The resulting cell suspension was centrifuged for 5 minutes at a speed of 1000 rpm and room temperature to obtain the cell pellet, which was resuspended in the 0.5% (w/v) NaAlg solution. The final bioink had cell concentration of 1×10^6 cells/ml and 5×10^6 cells/ml.

2.2. Experimental setup and conditions

Fig. 1 shows the experimental setup of the proposed bioink circulation-assisted inkjet printing system. It comprises of a customized bioink reservoir with active circulation, a pneumatic controller to optimize the back pressure, an inkjet dispenser with an orifice diameter of 120 μm, a waveform generator providing an excitation voltage signal to the inkjet dispenser, an imaging system to capture the droplet formation process, and a substrate container with the crosslinking agent of 2% (w/v) calcium chloride solution. The customized bioink reservoir with active circulation shown in Fig. 1 includes a bioink reservoir with inner diameter of 8 mm and volume capacity of 1.5 ml, a biocompatible silicone tube with inner diameter of 0.5 mm and length of 35 cm, which connects the top and bottom of the bioink reservoir, and a peristaltic pump enabling adjustment of the flow rates in the range of 0.002–2 ml/min. The peristaltic pump is equipped with a 10-roller rotor which extracts the bioink from the bottom of bioink reservoir and replenishes it to the top to achieve active circulation of the bioink within the reservoir. It is noted that the outlet end of the tube is located right above the bioink liquid level rather than being submerged into the bioink bulk to secure a consistent and holistic circulation within the bioink reservoir. Technically, circulating bioink from the top to the bottom of the bioink reservoir is difficult to realize in practical operation, because it requires continuous and precise control of the tube outlet level to match the decreasing bioink liquid level due to the bioink consumption during printing.

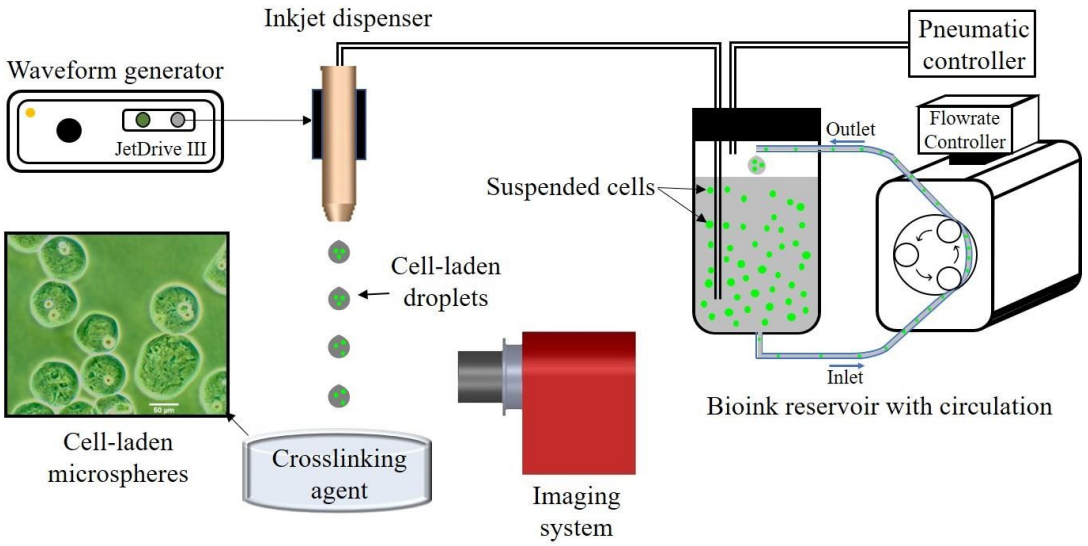

Fig. 1. Schematic diagram of inkjet bioprinting system with active bioink circulation

This study focuses on the effects of active bioink circulation on the cell sedimentation and aggregation in inkjet-based bioprinting. The major experimental conditions are summarized in Table 1. The circulation flow rate was in the range of 0.01–0.5 ml/min. The typical cell concentration in this study was 1×10^6 cells/ml, which is commonly used in 3D bioprinting [34]. The high cell concentration of 5×10^6 cells/ml, resulting in severe cell sedimentation and aggregation, was also selected to demonstrate the high effectiveness of the proposed active circulation approach. The printing time was in the range of 0–60 minutes with an interval of 20 minutes. The bioink containing 0.5% (w/v) NaAlg was selected due to the prominent cell sedimentation phenomenon [38]. The initial bioink volume was fixed to 1 ml. The process parameters of the applied excitation waveform were fixed as follows: excitation voltage 60 V, rise time 3 µs, dwell time 25 µs, fall time 5 µs, echo time 30 µs, and final rise time 3 µs.

Table 1. Major experimental conditions in this study

Experimental condition	**Unit**	**Value**
Circulation flow rate	ml/min	0.01, 0.05, 0.1, 0.5
NaAlg concentration	w/v	0.5%
Cell concentration	cells/ml	1×10^6, 5×10^6
Printing time	minutes	20, 40, 60
Bioink volume	ml	1

2.3. Cell concentration and aggregation quantification

The cell sedimentation was quantified through measuring the cell concentrations at the top and bottom of the bioink reservoir. 10 µl bioink sample was collected and added into a hemocytometer (Hausser Scientific, Horsham, PA) for measurement of the cell concentration. The cell aggregation is quantified by classifying it into three types depending on the aggregation level: individual cells without aggregation, small cell aggregates containing 2–4 cells, and large cell aggregates containing at least 5 cells. The percentage of individual cells was characterized as:

$$ic\% = \frac{\sum_{a=1} ab}{Total\ number\ of\ cells} \times 100\% \quad (1)$$

where a is 1 for individual cells, and b is the associated appearance frequency of individual cells. The percentage of the cells forming small aggregates was characterized as:

$$sa\% = \frac{\sum_{a=2}^{4} ab}{Total\ number\ of\ cells} \times 100\% \quad (2)$$

where a is in the range of 2–4 representing the cell number contained in the small aggregates, and b is the associated appearance frequency of small aggregates. The percentage of the cells forming large aggregates was characterized as:

$$la\% = \frac{\sum_{a=5}^{c} ab}{Total\ number\ of\ cells} \times 100\% \quad (3)$$

where c is the maximum cell number in the cell aggregates, a is in the range of 5–c representing the number of the cells in the large aggregates, and b is the associated appearance frequency of large aggregates.

2.4. Cell viability

A fluorescence assays consisting of calcein AM and ethidium homodimer III (Biotium, Fremont, CA) were utilized to assess the cell viability [39]. The protocol is as follows: (1) mixing calcein AM and ethidium homodimer III with Dulbecco's Modified Eagle Medium (DMEM, Sigma-16 Aldrich, St. Louis, MO) to make the staining solution; (2) adding the samples into the staining solution and incubating for 20 minutes in a humidified 5% CO_2 incubator at 37 ℃; and (3) imaging the stained cells using a fluorescence microscope (EVOS FL, Thermo Fisher Scientific, Waltham, MA). Calcein AM is membrane-permeant and emits strong green fluorescence for the living cells, and the ethidium homodimer III is membrane-impermeant and binds to DNA emitting red fluorescence. Cell viability is defined as a ratio of the number of living cells over the total number of cells.

2.5. Statistics

Data is shown in mean values ± standard deviation. To test the significance of difference among the different datasets, one-way analysis of variance (ANOVA) and Tukey multiple comparisons test were performed using the software R (R Core Team). $P < 0.05$ (*) represents the statistical significance.

2.6. Force and velocity analysis

Cell sedimentation phenomenon is mainly governed by the cell gravitational force, buoyant force, drag force. The detailed characterization of these forces can be found in our previous study [38]. Gravitational force and buoyant force are defined as follows, respectively:

$$G = \rho_{cell} V_{cell} g \quad (4)$$

$$F_B = \rho_f V_{cell} g \quad (5)$$

where ρ_{cell} is the cell density, ρ_f is the fluid density, g is gravitational acceleration, and V_{cell} is the volume of the cell. When the bioink is stationary, the suspended cells sediment to the bottom of the bioink reservoir because the cell gravitational force is greater than the cell buoyant force at initial. Drag force then comes into play when there is a relative motion between the cells and the

surrounding fluid. The drag force is the resistance force opposite to the motion of the cells relative to the surrounding fluid. It is calculated by the following formula [38, 40]:

$$F_D = \frac{1}{2}\rho_f v_c^2 C_d A \quad (6)$$

where v_c is the velocity of cells in motion relative to the surrounding fluid, C_d is the drag coefficient, and A is the cross-sectional area of the cells. The drag coefficient C_d is related to the Reynolds number Re, defined as $Re = \frac{\rho_f v_c D}{\mu}$, where D is the cell diameter, and μ is the dynamic viscosity of the fluid [40]. ρ_f, A, D, and μ are generally unaltered during the printing process and v_c is deemed to influence the magnitude of the drag force. At force equilibrium, the cell gravitational force is balanced by the cell buoyant force and drag force shown in Fig. 2(a). It was reported that the cell sedimentation velocity had no significant change during the sedimentation process [38]. For the bioink containing 0.5% (w/v) NaAlg, the cell sedimentation velocity at static fluid ($v_{c\text{-}s}$) is around 1.45 μm/s [38]. When the circulation is implemented, the peristaltic pump continuously transfers the bioink from the bottom to the top of the bioink reservoir with a fluid velocity v_f. In the bioink reservoir, the fluid velocity is downward. After force equilibrium, the cell gravitational force is balanced by the cell buoyant force and drag force. The cell velocity is $v_{cell} = v_f + v_{c\text{-}s}$ shown in Fig. 2(b). In the circulation tube, the fluid velocity is upward. After force equilibrium, the cell gravitational force is balanced by the cell buoyant force and drag force. The cell velocity is $v_{cell} = v_f - v_{c\text{-}s}$ shown in Fig. 2(c).

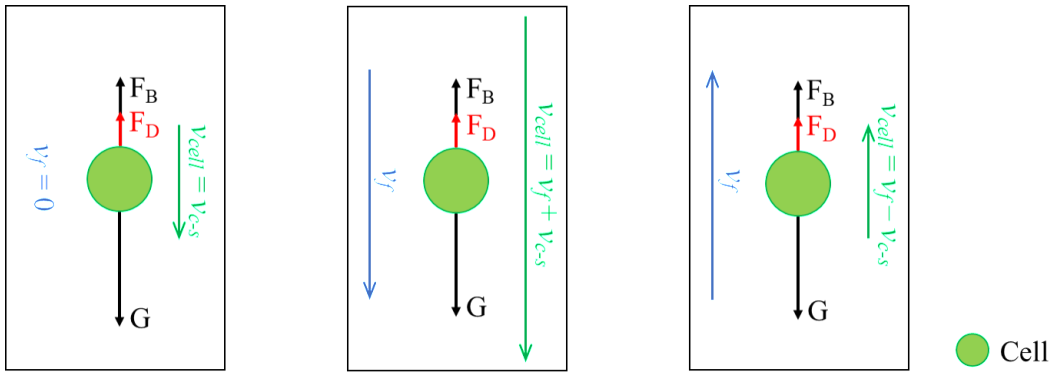

(a) (b) (c)

Fig. 2. Force and velocity analysis of cells at force equilibrium during cell sedimentation: (a) at static fluid, (b) in the bioink reservoir with a downward flow, and (c) in the circulation tube with an upward flow

3. Results

In this study, we incorporate the active circulation into the bioink reservoir to mitigate the cell sedimentation and aggregation. Section 4.1 presents a cell sedimentation model to predict the local cell concentrations at the top and bottom of the bioink reservoir. Section 4.2 compares the cell sedimentation and aggregation with and without the active bioink circulation, demonstrating the effectiveness of the proposed approach. Section 4.3 quantitatively investigates the effects of the circulation flow rate on the cell sedimentation and aggregation. Section 4.4 investigates the effects

of the circulation flow rate on the cell sedimentation and aggregation for high cell concentration, demonstrating the wide applicability/adaptability of the proposed approach.

3.1. Circulation model

It is noted that the proposed circulation model is based on sedimentation of individual cells without aggregation [38]. During the circulation, the applied flow rate is Q_f. The fluid velocities in the bioink reservoir and the circulation tube can be calculated, respectively, as:

$$v_{f-r} = \frac{Q_f}{A_r} \tag{7}$$

$$v_{f-t} = \frac{Q_f}{A_t} \tag{8}$$

where $v_{f\text{-}r}$ is the fluid velocity in the bioink reservoir, A_r is the cross-sectional area of the bioink reservoir, $v_{f\text{-}t}$ is the fluid velocity in the circulation tube, and A_t is the cross-sectional area of the tube. The cell velocities in the bioink reservoir and the circulation tube are calculated, respectively, as:

$$v_{c-r} = v_{f-r} + v_{c-s} \tag{9}$$

$$v_{c-t} = v_{f-t} - v_{c-s} \tag{10}$$

where $v_{c\text{-}r}$ is the cell velocity in the bioink reservoir, and $v_{c\text{-}t}$ is the cell velocity in the circulation tube. The flow rates selected in this study is 0.01–1 ml/min. The calculated fluid velocity in the circulation tube is $v_{f\text{-}t}$ = 1–100 mm/s, which is significantly higher than the cell sedimentation velocity in the static flow $v_{c\text{-}s}$ = 1.45 μm/s. Hence, the fluid velocity and cell velocity in the circulation tube have no significant difference. The cell sedimentation in the circulation tube is neglected. However, the magnitude of the fluid velocity in the bioink reservoir is $v_{f\text{-}r}$ = 1–100 μm/s, which is comparable to $v_{c\text{-}s}$. Therefore, the modeling in this study focuses on the cell sedimentation within the bioink reservoir.

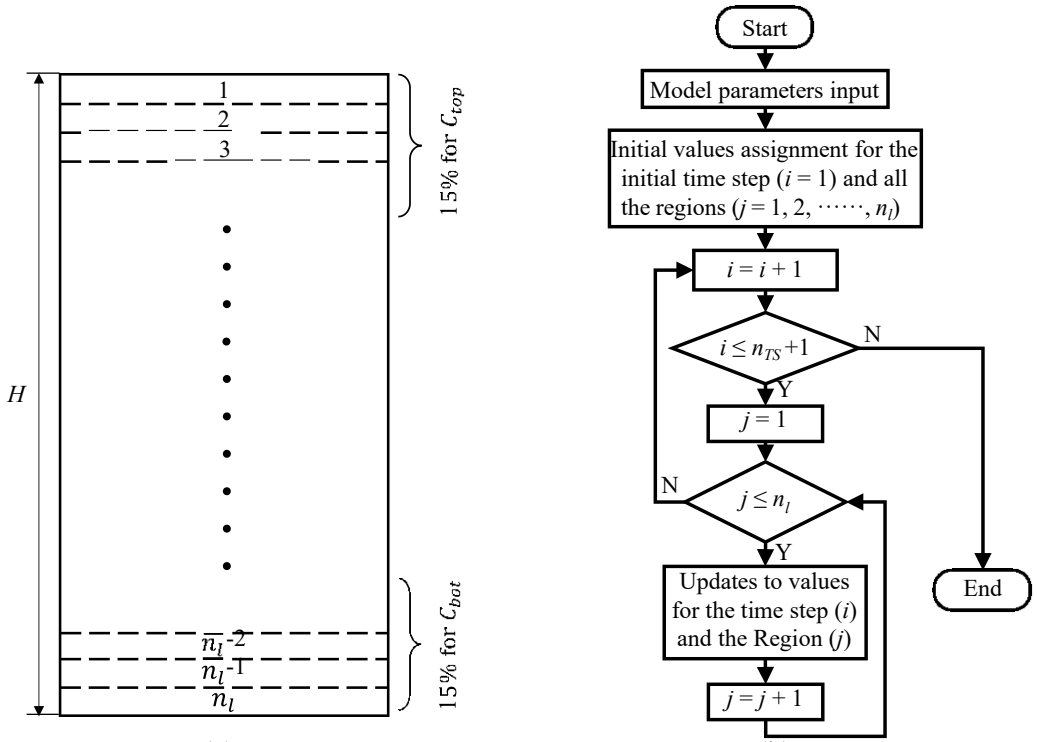

(a) (b)

Fig. 3. (a) Regions are divided and numbered within the bioink reservoir, and (b) flow chart shows the iteration with the time step for each divided region where n_{TS} is the number of the iteration

Within an infinitesimal space, the ratio of the number of cells at the end and the beginning of the time period can be calculated using the following equation:

$$\frac{nc_{end}}{nc_{start}} = \frac{C \cdot A_r \cdot v_{f-r} \cdot t - C \cdot A_r \cdot v_{c-s} \cdot t}{C \cdot A_r \cdot v_{f-r} \cdot t} = \frac{v_{f-r} - v_{c-s}}{v_{f-r}} \tag{11}$$

Where nc_{end} is the number of cells at the end of the time step, nc_{start} is the number of cells at the beginning of the time step, C is the cell concentration within the space, and t is the time step. The height of the bioink reservoir is H, and the bioink reservoir is divided into n_l regions with a height of H/n_l. Each region is numbered shown in Fig. 3(a). The model is based on iteration with the time step for each divided region. The number of cells in Region 1 at the end of the time step can be calculated as:

$$nc(i+1,1) = nc(i,1) \cdot \frac{v_{f-r} - v_{c-s}}{v_{f-r}} \tag{12}$$

The number of cells in Regions 2–n_l-1 at the end of the time step can be calculated as:

$$nc(i+1,j) = nc(i,j) \cdot \frac{v_{f-r} - v_{c-s}}{v_{f-r}} + nc(i,j-1) - nc(i+1,j-1) \tag{13}$$

where i is the i^{th} time step, and j is the number of the region. The number of cells in Region n_l at the end of the time step can be calculated as:

$$nc(i+1,n_l) = nc(i,n_l) \cdot \frac{v_{f-r}}{v_{f-r}} + nc(i,n_l-1) - nc(i+1,n_l-1) \tag{14}$$

During iteration, the total number of cells in the bioink reservoir remains constant. The measurement area of cell concentration is the 15% of the bioink reservoir at the top and the bottom. The cell concentrations at the top and the bottom of the bioink reservoir are calculated using the following equations, respectively:

$$C_{top} = \frac{\sum_{j=1}^{0.15n_l} nc(n_{TS},j)}{0.15 \cdot A_r \cdot h} \quad (15)$$

$$C_{bot} = \frac{\sum_{j=0.85n_l}^{n_l} nc(n_{TS},j)}{0.15 \cdot A_r \cdot h} \quad (16)$$

where n_{TS} is the time step number. The flow chart in Fig. 3(b) shows the iteration with the time step for each divided region. The parameters used in the model are listed in Table 2.

Table 2. Parameters used for cell sedimentation with active circulation model

Model Parameters	**Unit**	**Value**
Radius of bioink reservoir	mm	4
System flow rate (Q_f)	ml/min	0.01–0.5
Relative cell sedimentation velocity ($v_{c\text{-}s}$)	μm/s	1.45
Fluid velocity within bioink reservoir ($v_{f\text{-}r}$)	mm/s	$3.32–166\times10^{-3}$
Height of bioink (H)	mm	19.9
Number of regions (n_l)		10000
Total printing time	s	3600
Time step (t)	s	1.37

3.2. Comparison of the cell sedimentation and aggregation with and without the active bioink circulation

Cell sedimentation and aggregation are compared using the inkjet printing system with and without the active circulation. The top and the bottom of the bioink reservoir are selected to quantify the cell sedimentation and aggregation, representing the uniformity of the bioink the reservoir. The cell sedimentation is quantified using the local cell concentrations at the top and bottom of the bioink reservoir. The cell aggregation is quantified using the percentage of the three types of the cell aggregates at the bottom of the bioink reservoir including individual cells without aggregation, small aggregates with 2–4 cells, and large aggregates with at least 5 cells. Two circulation conditions are applied as with active circulation of 0.5 ml/min and without active circulation. The bioink contains 0.5 (w/v) NaAlg and a cell concentration of 1×10^6 cells/ml.

In Fig. 4(a), it shows the comparison of the cell concentrations at the top and bottom of the bioink reservoir with and without the active circulation. Without the active circulation, as the printing time increases from 0 to 20 to 40 to 60 minutes, the cell concentration on the top of the bioink reservoir decreases significantly from 1.00 to 0.29 to 0.1 to 0.07×10^6 cells/ml mainly due to cell sedimentation. After the 60 minutes, the cell concentration on the top is significantly reduced by 93%. Very few cells remain on the top of the bioink reservoir. On the contrary, as the printing time increases from 0 to 20 to 40 to 60 minutes, the cell concentration at the bottom of the bioink reservoir increases significantly from 1.01 to 1.56 to 2.42 to 3.68×10^6 cells/ml mainly due to cell sedimentation. After the 60 minutes, the cell concentration at the bottom significantly increased by nearly 268%. Numerous cells sediment to the bottom of the bioink reservoir, significantly

increasing the local cell concentration. The highly non-uniform bioink due to the cell sedimentation is demonstrated by comparing the local cell concentrations at the top 0.07 × 10^6 cells/ml and at the bottom 3.68 × 10^6 cells/ml. With the active circulation of 0.5 ml/min, as the printing time increases from 0 to 20 to 40 to 60 minutes, the cell concentration at the top of the bioink reservoir slightly decreases from 1.00 to 0.99 to 0.97 to 0.96 × 10^6 cells/ml, and the cell concentration at the bottom of the bioink reservoir slightly increases from 1.01 to 1.04 to 1.06 to 1.06 × 10^6 cells/ml. After the printing time of 60 minutes, the cell concentrations at the top and the bottom are 0.96 × 10^6 cells/ml and 1.06 × 10^6 cells/ml, respectively. The bioink within the reservoir is relatively uniform in the cell concentration, which demonstrates the high effectiveness of the active circulation to mitigate the cell sedimentation.

Fig. 4(b) shows the comparison of the cell aggregation at the bottom of the bioink reservoir with and without the active circulation. Without the active circulation, as the printing time increases from 0 to 20 to 40 to 60 minutes, the percentage of the individual cells without aggregation decreases significantly from 96.68 to 80.00 to 60.99 to 32.83%, while that of the small aggregates increases significantly from 3.32 to 19.21 to 37.63 to 49.24%, and that of the large aggregates also increases significantly from 0.00 to 0.79 to 1.38 to 17.93%. After 60 minutes, the percentage of the individual cells is only 32.83%, and that of the small aggregates and that of the large aggregates are 49.24% and 17.93%, respectively. The distribution of three types of cell aggregates demonstrates the significance of the cell aggregation challenge in 3D bioprinting. However, with the active circulation of 0.5 ml/min, as the printing time increases from 0 to 20 to 40 to 60 minutes, the percentage of the individual cells without aggregation decreases from 96.36 to 95.21 to 91.20 to 86.79%, while that of the small aggregates increases from 3.64 to 4.50 to 8.22 to 10.71%, and that of the large aggregates slightly increases from 0.00 to 0.29 to 0.58 to 2.50%. After 60 minutes, the percentage of the individual cells is 86.79%, and that of the small and that of the large aggregates are 10.71% and 2.50%, respectively. In comparison, the percentages of the cell aggregates are 67.17% without the active circulation and 13.21% with the active circulation. The formation of cell aggregates within the bioink reservoir is significantly suppressed, which demonstrates the high effectiveness of the active bioink circulation to mitigate the cell aggregation.

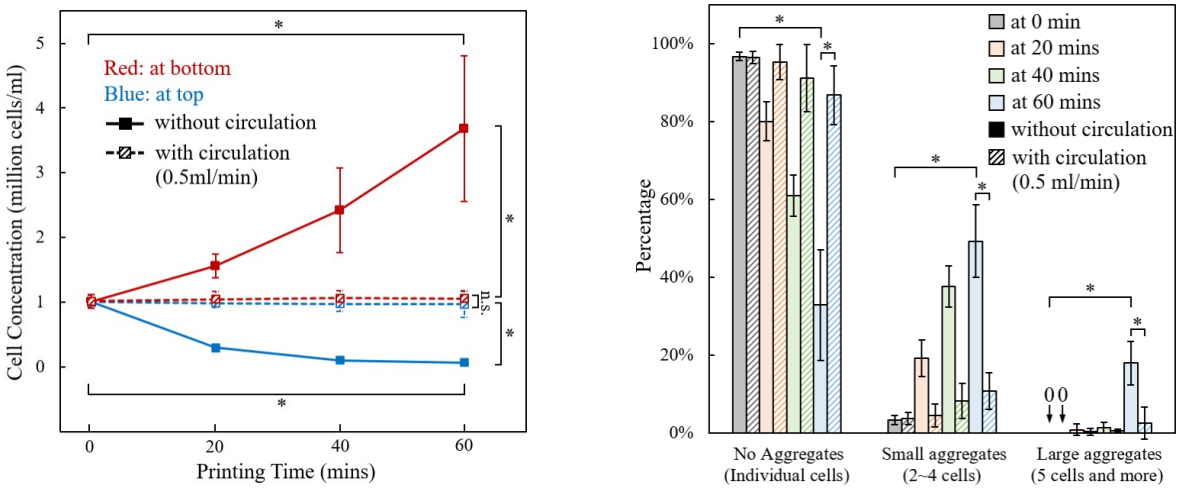

(a) (b)

Fig. 4. Experimental quantifications of cell sedimentation and cell aggregation at the cell concentration of 1 × 10^6 cells/ml over 60 minutes: (a) Comparison of local cell concentrations at

the top and bottom of the bioink reservoir with and without circulation, and (b) Comparison of cell aggregation at the bottom of the bioink reservoir with and without circulation

3.3. Effects of circulation flow rate on cell sedimentation and aggregation

Fig. 5(a) shows the effect of active bioink circulation flow rate on cell sedimentation at the top and the bottom of the bioink reservoir at 60 minutes. Initially, the cell concentration is 1×10^6 cells/ml for both the top and bottom. As the flow rate increases from 0 to 0.01 to 0.05 to 0.1 to 0.5 ml/min, the measured cell concentration at the top increases significantly from 0.07 to 0.38 to 0.79 to 0.96 to 0.96×10^6 cells/ml, while that at the bottom decreases significantly from 3.68 to 1.60 to 1.16 to 1.06 to 1.06×10^6 cells/ml. Moreover, the mitigation of the cell sedimentation at the flow rate of 0–0.05 ml/min is more significant than that at the flow rate of 0.05–0.5 ml/min. As the flow rate increases from 0 to 0.05 ml/min, the respective cell concentration at the top and that at the bottom are significantly increased by more than ten times and decreased by 68%, while there is only 23% and 9% improvement, respectively, as the flow rate increases from 0.05 to 0.5 ml/min. This indicates that the effectiveness of the circulation on the cell sedimentation is dependent on the flow rate. Large flow rate results in slow increments in effectiveness. In addition, the proposed model in Section 3.1 is utilized to predict the local cell concentrations at the top and bottom of the bioink reservoir under different circulation flow rates. As the flow rate increases from 0.01 to 0.05 to 0.1 to 0.5 ml/min, the predicted cell concentration at the top increases from 0.24 to 0.85 to 0.92 to 0.99 $\times 10^6$ cells/ml, while the predicted cell concentration at the bottom decreases from 1.76 to 1.15 to 1.08 to 1.02 cells/ml. The comparison of the predictions by the model and the experimental results shows good agreement. It is noted that the predicted top cell concentration at flow rate of 0.01 ml/min is less than the experimental results, and the predicted bottom cell concentration bottom at flow rate of 0.01 ml/min is greater than the experimental results. The main reasons are the variation of the cell sedimentation velocity and the formation of cell aggregates.

Fig. 5(b) shows the effect of active bioink circulation flow rate on cell aggregation at the bottom of the bioink reservoir at 60 minutes. As the flow rate increases from 0 to 0.01 to 0.05 to 0.1 to 0.5 ml/min, the measured percentage of the individual cells without aggregation increases significantly from 32.83% to 47.81% to 77.80% to 85.14% to 86.79%, while the percentage of cells forming the small aggregates decreases significantly from 49.24% to 33.87% to 20.48% to 14.03% to 10.71%. At the flow rate of 0–0.01 ml/min the percentage of cells forming the large aggregates is around 18%, and at the flow rate of 0.01–0.5 ml/min the percentage of cells forming the large aggregates is significantly reduced to less than 2.6%. Regarding improvement, comparing the flow rate increase from 0 to 0.05 ml/min with that from 0.05 to 0.5 ml/min, the former improvement percentage of the individual cells without aggregation is 44.97% while the latter is only 8.99%. The respective improvement percentages for the cells forming small aggregates are 28.76% and 9.77% and that for the cells forming large aggregates are 16.21% and -0.78%. Generally, large flow rate results in slow increments in effectiveness. Although the effectiveness of the circulation on the cell aggregation is dependent on the flow rate, it is more complex than that on the cell sedimentation because of the implicit transformation between the small aggregates and the large aggregates.

Fig. 5(c) shows the mitigation effectiveness percentage on cell sedimentation. The local cell concentrations at the top and bottom of the bioink reservoir with different circulation flow rates are normalized based on those without circulation. It is seen that as the flow rate increases from

0.01 to 0.05 to 0.1 to 0.5 ml/min, the mitigation effectiveness on cell sedimentation at the top increases significantly from 33.38% to 77.38% to 95.68% to 96.26%, and that at the bottom also increases significantly from 77.71% to 94.01% to 97.82% to 98.09%. This observation indicates that the mitigation effectiveness on the cell sedimentation at the top is more pronounced that that at the bottom. This is mainly due to the circulation of the bioink from the bottom to the top, significantly replenishing the total cell number at the top of the bioink reservoir. In addition, the proposed model in Section 3.1 is utilized to predict the mitigation effectiveness on local cell concentrations at the top and bottom of the bioink reservoir under different circulation flow rates. As the flow rate increases from 0.01 to 0.05 to 0.1 to 0.5 ml/min, the predicted mitigation effectiveness on cell sedimentation at the top increases significantly from 18.09% to 83.48% to 91.65% to 98.19%, and the predicted mitigation effectiveness on cell sedimentation at the bottom increases significantly from 71.51% to 94.35% to 97.21% to 99.49%. The model prediction generally agrees well with the experimental results, except for a slight underestimation at the low flow rates. The main reasons are the variation of the cell sedimentation velocity and the formation of cell aggregates. Moreover, with the increase of the circulation flow rate, the mitigation effectiveness generally increases and approaches to 100%. At the flow rate of 0.1 ml/min, the mitigation effectiveness is around 95%, and after 0.1 ml/min the improvement in the mitigation effectiveness becomes very slow. The results regarding the mitigation effectiveness on the cell sedimentation demonstrates the high effectiveness of the proposed active circulation in mitigating cell sedimentation.

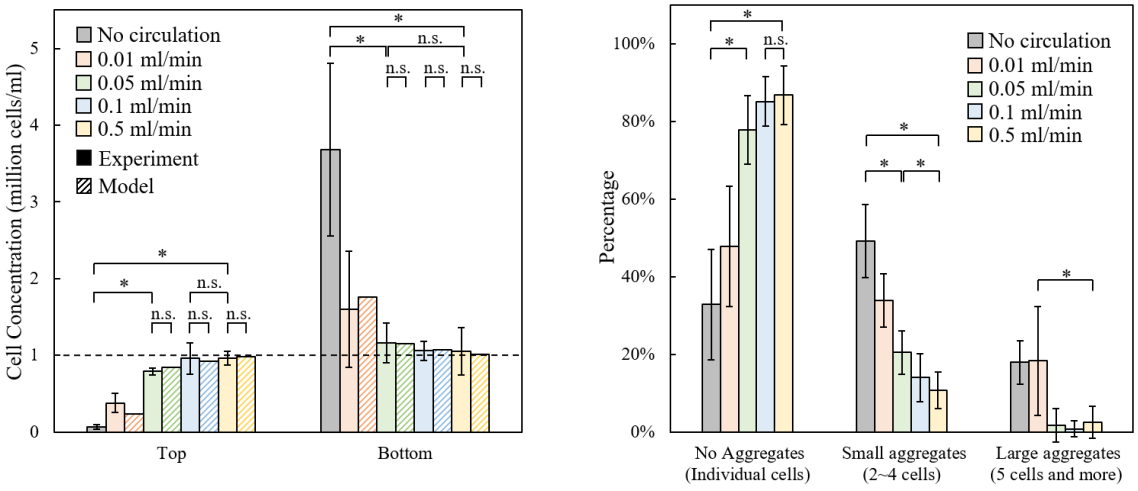

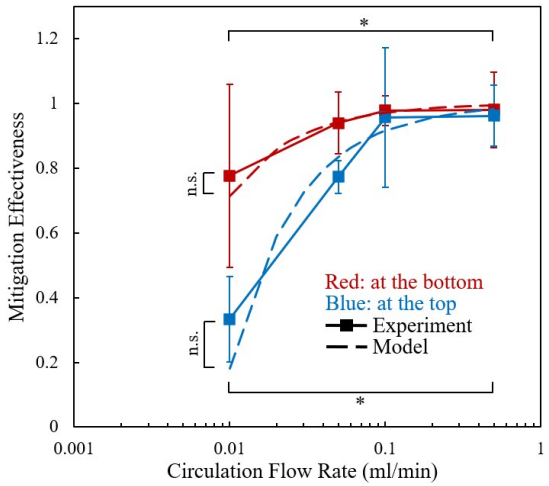

(c)

Fig. 5. Effects of bioink circulation flow rate on (a) cell sedimentation at 60 minutes, (b) cell aggregation at 60 minutes, and (c) mitigation effectiveness of cell sedimentation at 60 minutes

3.4. Circulation effects on cell sedimentation and aggregation using bioink with high cell concentration

To investigate the mitigation effectiveness of active bioink circulation on cell sedimentation and aggregation with high cell concentration, 5×10^6 cells/ml was selected at the circulation flow rate of 0.5 ml/min. Fig. 6(a) shows the comparison of the cell concentrations at the top and the bottom of the bioink reservoir with and without the active circulation. Without the active circulation, as the printing time increases from 0 to 20 to 40 to 60 minutes, the cell concentration at the top decreases significantly from 5.09 to 1.34 to 0.34 to 0.23×10^6 cells/ml, while the cell concentration at the bottom increases significantly from 5.07 to 9.03 to 18.75 to 28.75×10^6 cells/ml. After 60 minutes, the cell concentration on the top is reduced by 95%, while the cell concentration at the bottom is increased by nearly 467%. A large number of cells sediment to the bottom of the bioink reservoir, significantly increasing the local cell concentration. The bioink in the reservoir is highly non-uniform due to cell sedimentation by comparing the local cell concentrations at the top—0.2×10^6 cells/ml and at the bottom—28.75×10^6 cells/ml. With the active circulation of 0.5 ml/min, as the printing time increases from 0 to 20 to 40 to 60 minutes, the cell concentration at the top decreases from 4.98 to 4.68 to 4.54 to 4.13×10^6 cells/ml, and the cell concentration at the bottom increases from 5.11 to 5.48 to 5.93 to 6.66×10^6 cells/ml. After 60 minutes, the cell concentrations at the top and the bottom are 4.13×10^6 cells/ml and 6.66×10^6 cells/ml, respectively. The uniformity of the bioink in the reservoir is significantly improved at the 60 minutes mainly due to the active circulation, which demonstrates the effectiveness of the active circulation to mitigate the cell sedimentation with high cell concentration.

Fig. 6(b) shows the comparison of the cell aggregation at the bottom of the bioink reservoir with and without the active circulation. Without the active circulation, as the printing time increases from 0 to 20 to 40 to 60 minutes, the percentage of the individual cells without aggregation decreases significantly from 70.88% to 31.17% to 6.67% to 2.62%, while the percentage of cells forming the small aggregates increases from 27.77% to 48.10% and then decreases to 28.00% to 18.26%, and the percentage of cells forming large aggregates increases significantly from 1.35% to 20.74% to 65.33% to 79.13%. After 60 minutes, the percentage of the individual cells is only

2.61%, while the percentages of cells forming the small and large aggregates are 18.26% and 79.13%, respectively. In comparison, with the active circulation of 0.5 ml/min, as the printing time increases from 0 to 20 to 40 to 60 minutes, the percentage of the individual cells without aggregation decreases from 72.39% to 67.89% to 60.98% to 48.06%, while the percentage of cells forming small aggregates increases from 25.25% to 27.18% to 29.17% to 29.85%, and the percentage of cells forming the large aggregates increases from 1.52% to 4.93% to 9.84% to 22.09%. After 60 minutes, the percentage of the individual cells is 48.06%, and the percentages of cells forming the small and large aggregates are 29.85% and 22.09%, respectively. The percentage of the cells forming aggregates are 97.38% without the active circulation compared to 51.94% with the active circulation. With the active circulation, the formation of cell aggregates within the bioink reservoir is significantly reduced by almost 47%, which demonstrates the effectiveness of the active circulation to mitigate the cell aggregation even with a high cell concentration. It is noted that more cell aggregates are observed in this case with cell concentration of 5×10^6 cells/ml compared to the case with cell concentration of 1×10^6 cells/ml. This is mainly because the distance between adjacent cells is smaller, and it is much easier to form cell aggregates through cell-cell interaction at a high cell concentration.

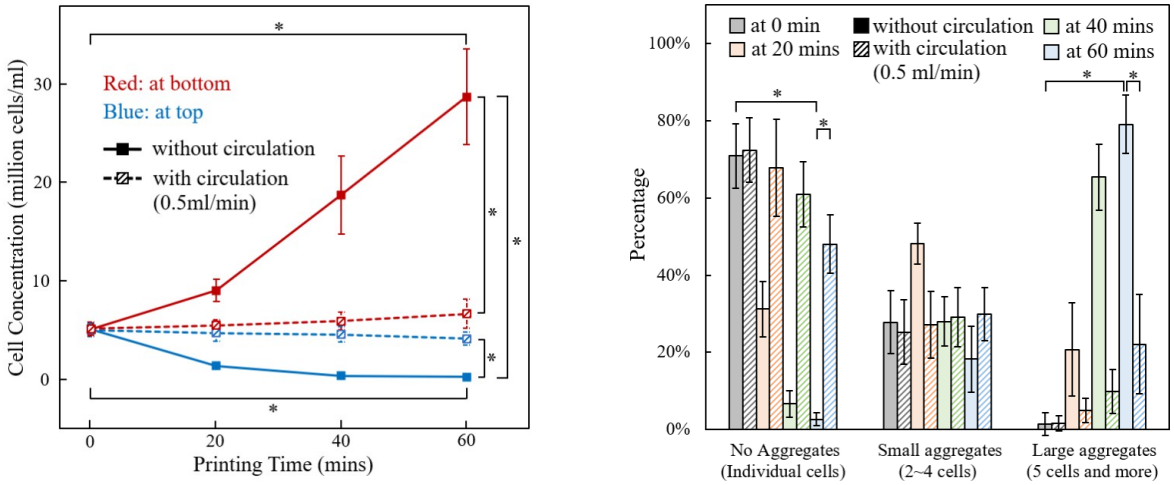

(a) (b)

Fig. 6. Experimental quantifications of cell sedimentation and cell aggregation at the cell concentration of 5×10^6 cells/ml over 60 minutes: (a) Comparison of local cell concentrations at the top and bottom of the bioink reservoir with and without circulation, and (b) Comparison of cell aggregation with and without circulation

4. Discussions

4.1. Bubble formation at high circulation flow rates

General speaking, high flow rates improve the mitigation performance regarding the cell aggregation during the printing process. However, excessively high flow rates may result in large velocity fields at the top of the bioink reservoir, where the circulated bioink impacts with the bulk bioink. During the impaction, small bubbles may be generated. When the bubbles reach the nozzle, they are enlarged under the propagation of the pressure waves inside the nozzle. The size of the bubbles could become large enough to block the nozzle shown in Fig. 7. In our experiments, we observed that the bubble started to form at the flow rate > 0.5 ml/min. At the flow rate 0.5–1 ml/min, small bubbles are formed sometimes, which slightly affects the nozzle behaviors. At the

flow rate > 1 ml/min, the bubble formation is a significant issue to affect the nozzle behaviors. The optimal flow rate for the bioink with low cell concentration is recommended as 0.1–0.5 ml/min. It is noted that this recommended flow rate is also affected by the remaining volume of the bioink within the reservoir. With the printing time, the volume of the bioink within the reservoir decreases since some of the bioink is ejected out to form cell-laden microspheres. The height between the outlet of the circulation tube and the bioink surface is larger. The recommended flow rate may decrease slightly with the printing time considering the dynamic decrease of the bioink volume with the printing time.

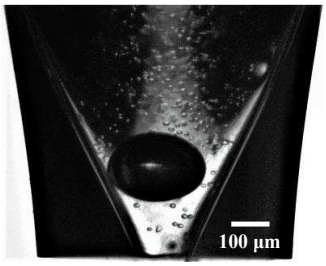

Fig. 7. Nozzle blocked by the generated bubble under circulation flow rates higher than 0.5 ml/min

4.2. Cell aggregation within nozzle

The previous results section investigates the cell aggregation with and without the active circulation within the bioink reservoir. After the bioink is transferred from the reservoir to the nozzle, this section focuses on the cell aggregation with and without the active circulation within the nozzle during the printing. Fig. 8 shows the cell aggregation with and without the active circulation within the nozzle during the printing. Two bioink is used with a low cell concentration of 1×10^6 cells/ml and a high cell concentration of 5×10^6 cells/ml. It is seen that at the printing time of 0 minutes the cells are uniformly dispersed inside the nozzle. At the printing time of 20 minutes for low cell concentration and 10 minutes for high cell concentration, the cell aggregation becomes prominent without the active circulation. For the low cell concentration, two large cell aggregates are formed in Fig. 8 containing more than 10 cells. The cell aggregates appear in the vicinity of the nozzle centerline due to the weak shear-thinning effect of the bioink [41]. Due to the formation of the cell aggregates, the bioink inside the nozzle becomes highly non-uniform. The droplet formation process is unstable, which makes it extremely difficult to precisely control the printing quality of the fabricated 3D structures. Due to the low cell concentration, the cell aggregate size is relatively small, and the nozzle blockage is not observed. For the high cell concentration, the cell aggregation is severe, and more large cell aggregates are observed. Sometimes, the largest cell aggregate contains more than 100 cells shown in Fig. 8. The size of the cell aggregate is even larger than the nozzle orifice size of 120 μm, and the nozzle orifice is blocked. However, with the active circulation of 0.5 ml/min flow rate, only few cell aggregates are observed for both cases shown in Fig. 8. Similar to the images at the printing time of 0 minutes, the cells are still uniformly dispersed inside the nozzle at the printing time of 20 minutes for the low cell concentration and 10 minutes for the high cell concentrations.

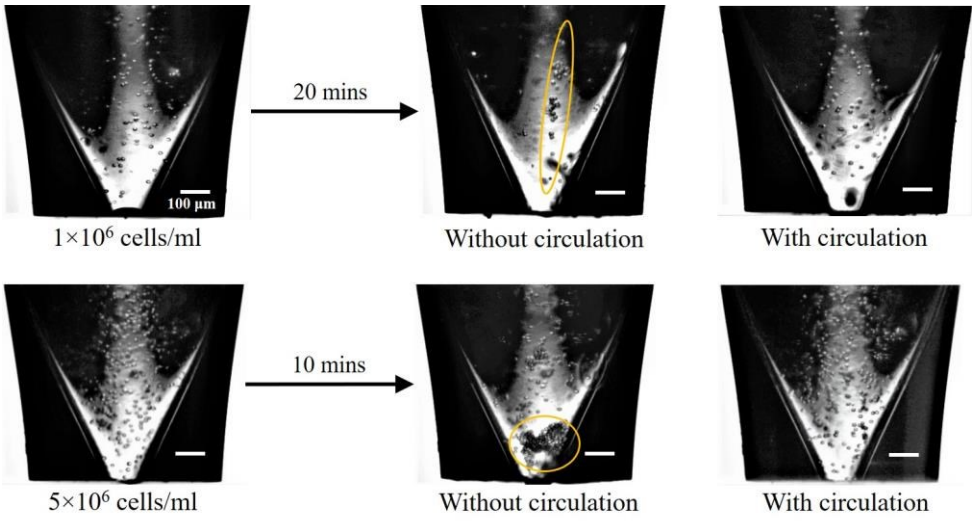

Fig. 8. Cell distribution within nozzle during inkjet printing of bioink with low and high cell concentrations without/with active circulation. The cell aggregation is highlighted

4.3. Cell viability

Cell viability is assessed using a fluorescence assay. Calcein AM is membrane-permeant and emits strong green fluorescence for the living cells, and the ethidium homodimer III is membrane-impermeant and binds to DNA emitting red fluorescence. Fig. 9 shows the cell viability assessment at the maximum flow rate of 0.5 ml/min using the bioink containing different cell concentrations. The maximum flow rate 0.5 ml/min is selected representing the largest shear stress as well as the corresponding maximum cell damage due to the active circulation. It is seen that the cell viability is around 99% at the printing time of 0 minutes. After the printing time of 60 minutes, the cell viability without circulation is around 95.5% and the cell viability with circulation is around 92.6%. The mild cell damage during the active circulation is mainly due to the shear stress within the small silicone tube connecting the top and bottom of the bioink reservoir. This cell viability results indicate that most cells survive during the active circulation and the associated cell damage is almost negligible.

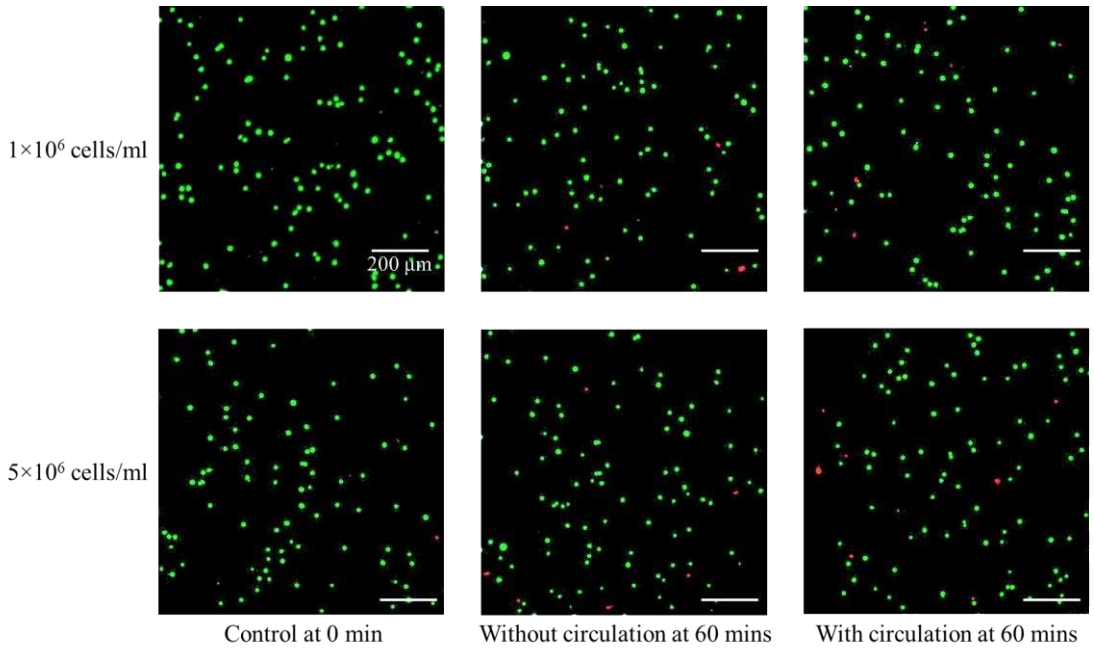

(a)

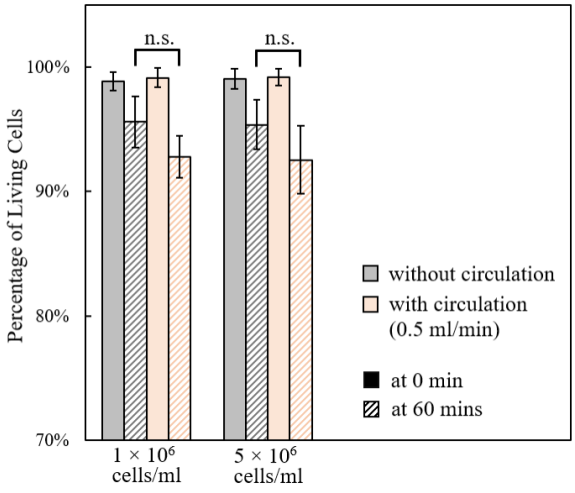

(b)

Fig. 9. (a) Representative fluorescence images of cell viability test and (b) cell viability assessment. Two bioink cell concentrations are selected as 1×10^6 cells/ml for low cell concentration and 5×10^6 cells/ml for high cell concentration. The other conditions are fixed as flow rate of 0.5 ml/min and NaAlg concentration of 0.5% (w/v).

4.4. Comparison of cell aggregation mitigation approaches

There are two approaches to mitigate cell sedimentation and aggregation in the literature: neutral buoyancy and active stirring. In neutral buoyancy, the gravitational force of the suspended cells is exactly balanced by the buoyant force and there is no relative motion between the cells and the biomaterial solution. Normally, the gravitational force of cells is greater than the buoyant force, resulting in cell sedimentation. In order to achieve the neutral buoyancy, the fluid density of the biomaterial solution must be increased, which can be done by increasing the biomaterial

concentration or adding extra biocompatible materials [25, 31, 38]. The advantages include no further modification of experimental setup and no extra shear stress in the bioink reservoir. However, this approach requires careful formulation to achieve the neutral buoyancy. The rheological properties may change due to addition of extra biomaterials, resulting in poor printing performance and nozzle clogging [30, 41]. Moreover, it is extremely difficult to accommodate multiple cell types in the bioink to achieve neutral buoyancy, because different types of cells have different cell mass densities. In active stirring, it utilizes magnetic-driven stir bar or axial flow impeller to physically agitate the bioink [32, 33]. This approach doesn't change the bioink rheological properties and can easily accommodate multiple types of cells. However, active stirring requires internal/external mounted stirrers/impellers with associated control module. Active stirring introduces high shear stress, which may damage cells. For example, the continuous stirring at a speed of 120 rpm was reported to decrease the cell viability from around 99% to 75% after 50-minute printing [33]. Moreover, the stirrers/impellers only stay at the bottom of the bioink reservoir for local agitation instead of holistic agitation. For the active circulation in this study, the important advantages include no alterations of bioink rheological properties, easy accommodation of multiple types of cells, holistic agitation, and high cell viability. Only one drawback is implementation of the circulation module. In summary, we believe that the proposed active circulation approach is an effective and efficient approach with superior performance in mitigating cell sedimentation and aggregation in 3D bioprinting.

5. Conclusions and future work

The bioink used for 3D bioprinting is composed of biological materials and cells. During the printing process, the cells suspended in the bioink sediment due to the dominant gravitational force. Once the distance between adjacent cells becomes small enough, the cells adhere with each other to form the cell aggregates through cell-cell interaction. The formation of cell aggregates induced by the cell sedimentation plays a critical role in the printing reliability and performance, which have been widely recognized as a significant challenge in 3D bioprinting. In this study, we incorporated the active circulation into the bioink reservoir to mitigate the cell sedimentation and aggregation. The cell sedimentation has been modeled based on iteration with the time step for each divided region of the bioink reservoir. Moreover, the effects of circulation flow rate on the cell sedimentation and aggregation have been investigated and the effectiveness of the proposed circulation-assisted approach for bioink with both low and high cell concentrations have been demonstrated. The main conclusions are as follow: (1) For the low cell concentration of 1×10^6 cells/ml, without the active circulation, the respective cell concentrations at the top and bottom of the bioink reservoir are 0.07×10^6 and 3.68×10^6 cells/ml at 60 minutes mainly due to cell sedimentation, while they are 0.96×10^6 and 1.06×10^6 cells/ml with the active circulation of 0.5 ml/min, demonstrating the high effectiveness of the active bioink circulation to mitigate the cell sedimentation. The percentages of the cell aggregates are 67.17% without the active circulation and 13.21% with the active circulation, demonstrating the high effectiveness of the active bioink circulation to mitigate the cell aggregation; (2) As the flow rate increases from 0 to 0.5 ml/min, the cell concentration at the top increases significantly from 0.07 to 0.96×10^6 cells/ml, while that at the bottom decreases significantly from 3.68 to 1.06×10^6 cells/ml. As the flow rate increases from 0 to 0.5 ml/min, the percentage of the individual cells without aggregation increases significantly from 32.83% to 86.79%, while the percentage of cells forming the aggregates decreases significantly from 67.17% to 13.21%. As the flow rate increases from 0.01 to 0.5 ml/min, the mitigation effectiveness on cell sedimentation at the top increases significantly from 33.38%

to 96.26%, and that at the bottom also increases significantly from 77.71% to 98.09%. Large flow rate results in slow increments in effectiveness; and (3) For the high cell concentration of 5×10^6 cells/ml, without the active circulation, the cell concentrations at the top and bottom of the bioink reservoir are 0.23×10^6 and 28.75×10^6 cells/ml at 60 minutes mainly due to cell sedimentation, while they are 4.13×10^6 and 6.66×10^6 cells/ml with the active circulation of 0.5 ml/min. The percentages of the cell aggregates are 97.38% without the active circulation and 51.49% with the active circulation. This demonstrates the high effectiveness of the active bioink circulation to mitigate the cell sedimentation and cell aggregation with high cell concentration. Future work may include improvement of the proposed model by considering the cell aggregation effects and investigation of the proposed circulation-assisted approach for bioink with different types of cells and multiple types of cells.

Acknowledgement

This study is partially supported by the National Science Foundation (CMMI-1762282).

Reference

[1] Ford, S. L., 2014, "Additive manufacturing technology: potential implications for US manufacturing competitiveness," Journal of International Commerce & Economics, 6, p. 40.

[2] Krishnamoorthy, S., Zhang, Z., and Xu, C., 2020, "Guided cell migration on a graded micropillar substrate," Bio-Design and Manufacturing, 3(1), pp. 60–70.

[3] Hua, W., Mitchell, K., Raymond, L., Godina, B., Zhao, D., Zhou, W., and Jin, Y., 2021, "Fluid bath-assisted 3D printing for biomedical applications: from pre-to postprinting stages," ACS Biomaterials Science & Engineering, 7(10), pp. 4736–4756.

[4] Derby, B., 2012, "Printing and prototyping of tissues and scaffolds," Science, 338(6109), pp. 921–926.

[5] Song, K., Ren, B., Zhai, Y., Chai, W., and Huang, Y., 2021, "Effects of transglutaminase cross-linking process on printability of gelatin microgel-gelatin solution composite bioink," Biofabrication, 14(1), p. 015014.

[6] Mehesz, A. N., Brown, J., Hajdu, Z., Beaver, W., Da Silva, J., Visconti, R., Markwald, R., and Mironov, V., 2011, "Scalable robotic biofabrication of tissue spheroids," Biofabrication, 3(2), p. 025002.

[7] Compaan, A. M., Christensen, K., and Huang, Y., 2017, "Inkjet bioprinting of 3D silk fibroin cellular constructs using sacrificial alginate," ACS Biomaterials Science & Engineering, 3(8), pp. 1519–1526.

[8] Gao, G., Schilling, A. F., Hubbell, K., Yonezawa, T., Truong, D., Hong, Y., Dai, G., and Cui, X., 2015, "Improved properties of bone and cartilage tissue from 3D inkjet-bioprinted human mesenchymal stem cells by simultaneous deposition and photocrosslinking in PEG-GelMA," Biotechnology Letters, 37(11), pp. 2349–2355.

[9] Masaeli, E., Forster, V., Picaud, S., Karamali, F., Nasr-Esfahani, M. H., and Marquette, C., 2020, "Tissue engineering of retina through high resolution 3-dimensional inkjet bioprinting," Biofabrication, 12(2), p. 025006.

[10] Ozbolat, I. T., and Hospodiuk, M., 2016, "Current advances and future perspectives in extrusion-based bioprinting," Biomaterials, 76, pp. 321–343.

[11] Song, K., Zhang, D., Yin, J., and Huang, Y., 2021, "Computational study of extrusion bioprinting with jammed gelatin microgel-based composite ink," Additive Manufacturing, 41, p. 101963.

[12] Lawlor, K. T., Vanslambrouck, J. M., Higgins, J. W., Chambon, A., Bishard, K., Arndt, D., Er, P. X., Wilson, S. B., Howden, S. E., and Tan, K. S., 2021, "Cellular extrusion bioprinting improves kidney organoid reproducibility and conformation," Nature Materials, 20(2), pp. 260–271.
[13] Yan, J., Huang, Y., and Chrisey, D. B., 2012, "Laser-assisted printing of alginate long tubes and annular constructs," Biofabrication, 5(1), p. 015002.
[14] Sole-Gras, M., Xiong, R., Liang, C., Roorda, W., Yamaguchi, H., and Huang, Y., 2021, "Study of overlapping adjacent jets for effective laser-induced forward transfer printing," Journal of Manufacturing Science and Engineering, 143(4), p. 041001.
[15] Sorkio, A., Koch, L., Koivusalo, L., Deiwick, A., Miettinen, S., Chichkov, B., and Skottman, H., 2018, "Human stem cell based corneal tissue mimicking structures using laser-assisted 3D bioprinting and functional bioinks," Biomaterials, 171, pp. 57–71.
[16] Dababneh, A. B., and Ozbolat, I. T., 2014, "Bioprinting technology: a current state-of-the-art review," Journal of Manufacturing Science and Engineering, 136(6), p. 061016
[17] Hong, N., Yang, G. H., Lee, J., and Kim, G., 2018, "3D bioprinting and its in vivo applications," Journal of Biomedical Materials Research Part B: Applied Biomaterials, 106(1), pp. 444–459.
[18] Yin, J., Zhao, D., and Liu, J., 2019, "Trends on physical understanding of bioink printability," Bio-Design and Manufacturing, 2(1), pp. 50–54.
[19] Markstedt, K., Mantas, A., Tournier, I., Martínez Ávila, H., Hagg, D., and Gatenholm, P., 2015, "3D bioprinting human chondrocytes with nanocellulose–alginate bioink for cartilage tissue engineering applications," Biomacromolecules, 16(5), pp. 1489–1496.
[20] Diamantides, N., Dugopolski, C., Blahut, E., Kennedy, S., and Bonassar, L. J., 2019, "High density cell seeding affects the rheology and printability of collagen bioinks," Biofabrication, 11(4), p. 045016.
[21] Ko, Y.-G., and Kwon, O. H., 2020, "Reinforced gelatin-methacrylate hydrogels containing poly (lactic-co-glycolic acid) nanofiber fragments for 3D bioprinting," Journal of Industrial and Engineering Chemistry, 89, pp. 147–155.
[22] Chen, N., Zhu, K., Zhang, Y. S., Yan, S., Pan, T., Abudupataer, M., Yu, G., Alam, M. F., Wang, L., and Sun, X., 2019, "Hydrogel bioink with multilayered interfaces improves dispersibility of encapsulated cells in extrusion bioprinting," ACS Applied Materials & Interfaces, 11(34), pp. 30585–30595.
[23] Pepper, M. E., Seshadri, V., Burg, T. C., Burg, K. J., and Groff, R. E., 2012, "Characterizing the effects of cell settling on bioprinter output," Biofabrication, 4(1), p. 011001.
[24] Lorber, B., Hsiao, W.-K., Hutchings, I. M., and Martin, K. R., 2013, "Adult rat retinal ganglion cells and glia can be printed by piezoelectric inkjet printing," Biofabrication, 6(1), p. 015001.
[25] Chahal, D., Ahmadi, A., and Cheung, K. C., 2012, "Improving piezoelectric cell printing accuracy and reliability through neutral buoyancy of suspensions," Biotechnology and Bioengineering, 109(11), pp. 2932–2940.
[26] Skardal, A., Mack, D., Kapetanovic, E., Atala, A., Jackson, J. D., Yoo, J., and Soker, S., 2012, "Bioprinted amniotic fluid-derived stem cells accelerate healing of large skin wounds," Stem Cells Translational Medicine, 1(11), pp. 792–802.
[27] Cui, X., Gao, G., Yonezawa, T., and Dai, G., 2014, "Human cartilage tissue fabrication using three-dimensional inkjet printing technology," Journal of Visualized Experiments, 88, p. e51294.

[28] Liu, F., Liu, C., Chen, Q., Ao, Q., Tian, X., Fan, J., Tong, H., and Wang, X., 2018, "Progress in organ 3D bioprinting," International Journal of Bioprinting, 4(1), p. 128.
[29] Xu, H., Liu, J., Zhang, Z., and Xu, C., 2022, "Cell sedimentation during 3D bioprinting: a mini review," Bio-Design and Manufacturing, 5, pp. 617–626.
[30] Lee, A., Sudau, K., Ahn, K. H., Lee, S. J., and Willenbacher, N., 2012, "Optimization of experimental parameters to suppress nozzle clogging in inkjet printing," Industrial & Engineering Chemistry Research, 51(40), pp. 13195–13204.
[31] Hewes, S., Wong, A. D., and Searson, P. C., 2017, "Bioprinting microvessels using an inkjet printer," Bioprinting, 7, pp. 14–18.
[32] Dudman, J. P., Ferreira, A. M., Gentile, P., Wang, X., Ribeiro, R. D. C., Benning, M., and Dalgarno, K. W., 2020, "Reliable inkjet printing of chondrocytes and MSCs using reservoir agitation," Biofabrication, 12(4), p. 045024.
[33] Parsa, S., Gupta, M., Loizeau, F., and Cheung, K. C., 2010, "Effects of surfactant and gentle agitation on inkjet dispensing of living cells," Biofabrication, 2(2), p. 025003.
[34] Zhang, Z., Jin, Y., Yin, J., Xu, C., Xiong, R., Christensen, K., Ringeisen, B. R., Chrisey, D. B., and Huang, Y., 2018, "Evaluation of bioink printability for bioprinting applications," Applied Physics Reviews, 5(4), p. 041304.
[35] Murphy, S. V., and Atala, A., 2014, "3D bioprinting of tissues and organs," Nature Biotechnology, 32(8), pp. 773–785.
[36] Gungor-Ozkerim, P. S., Inci, I., Zhang, Y. S., Khademhosseini, A., and Dokmeci, M. R., 2018, "Bioinks for 3D bioprinting: an overview," Biomaterials Science, 6(5), pp. 915–946.
[37] Shahriar, M., Liu, J., Xu, H., Zhang, Z., and Xu, C., 2022, "Effects of corona treatment on cellular attachment and morphology on polydimethylsiloxane micropillar substrates," JOM, pp. 1–11.
[38] Xu, H., Zhang, Z., and Xu, C., 2019, "Sedimentation study of bioink containing living cells," Journal of Applied Physics, 125(11), p. 114901.
[39] Teixeira, B. N., Aprile, P., Mendonca, R. H., Kelly, D. J., and Thiré, R. M. d. S. M., 2019, "Evaluation of bone marrow stem cell response to PLA scaffolds manufactured by 3D printing and coated with polydopamine and type I collagen," Journal of Biomedical Materials Research Part B: Applied Biomaterials, 107(1), pp. 37–49.
[40] Singh, N., Kroells, M., Li, C., Ching, E., Ihme, M., Hogan, C. J., and Schwartzentruber, T. E., 2022, "General drag coefficient for flow over spherical particles," AIAA journal, 60(2), pp. 587–597.
[41] Xu, H., Martinez Salazar, D. M., Shahriar, M., and Xu, C., 2022, "Investigation and characterization of cell aggregation during and after inkjet-based bioprinting of cell-laden bioink," Journal of Manufacturing Science and Engineering, 144(10), p. 104501.